A novel approach to determining the hydrodynamic resistance of droplets in microchannels using active control and grey-box system identification

Marie Hébert[1*], Jan P. Huissoon[2] and Carolyn L. Ren[2]

[1]Département de génie mécanique, Université du Québec à Trois-Rivières, 3351, Boul. des Forges, Trois-Rivières, G8Z 4M3, Québec, Canada.

[2]Mechanical and Mechatronics Engineering Department, University of Waterloo, 200, University Avenue West, Waterloo, N2L 3G1, Ontario, Canada.

*Corresponding author(s). E-mail(s): marie.hebert@uqtr.ca;
Contributing authors: jph@uwaterloo.ca; c3ren@uwaterloo.ca;

Abstract

Inaccurate prediction of droplet hydrodynamic resistance has a profound impact on droplet chip performance and lengthens the iterative design process. Previous studies measuring droplet resistance use various approaches such as interface comparison to quantify flow rate, and pressure taps; all these methods are classified as passive. Although each study supports well their own findings, the wide variety of conditions such as channel geometry and use of surfactant in combination with the difficulty in quantifying the droplet resistance leads to poor consensus across the different studies. Overall guidelines would be broadly beneficial to the community, but are currently fairly crude, with a rule of thumb of 2 to 5 times resistance increase. The active droplet control platform previously developed enables a novel approach that is herein confirmed as promising. This proof-of-concept study focuses on verifying this approach that employs a system identification method to determine the hydrodynamic resistance of a channel containing a single droplet, from which the droplet resistance is retrieved. This method has the potential to be further applied to a large variety of conditions,

and most importantly, to non-Newtonian fluids once key limitations are overcome to improve measurement resolution. The current results qualitatively agree with the literature and demonstrate the promising future for this novel active approach to quantifying droplet resistance.

Keywords: Microfluidics, hydrodynamic resistance, system identification

1 Introduction

1.1 Motivation

Microfluidics has a wide range of applications in various fields such as water treatment[1], life biology[2], and material synthesis[3]. An expansive literature covers the different droplet manipulations that can be achieved individually using passive microfluidics (e.g. droplet generation, merging, synchronization, trapping)[4]. However, most–if not all–applications require multiple manipulations implemented in series. For example, a drug screening assay performed on a single microfluidic chip includes: two droplet generators in parallel followed by traps immobilizing the droplets to mix their content by the overlapping interface[5]. Multiple iterations of the design must be performed to eventually obtain the final functional device. The iteration process is time and resource-intensive even with relatively short prototyping processes such as polydimethylsiloxane (PDMS)-based soft lithography[6]. The main factors contributing to the design difficulties are the operational uncertainties (short time pressure pump variations), manufacturing uncertainties (PDMS swelling affecting height and width dimensions, manufacturing defects), and most importantly, the unclear *quantitative* effect of droplets on flow rate from their resistance.

The Hagen-Poiseuille law (Equation 1) relates the pressure drop and flow rate using the so-called hydraulic resistance [7]. For pressure-driven flow (i.e. for a fixed user-defined pressure drop between inlets), the flow rate of a single-phase liquid will be inversely proportional to the resistance. The flow rate quantifies the behaviour of the flow in the channel given the input (applied pressure) and system (resistance). Although the Hagen-Poiseuille law is a simple equation, the response of micro-channel networks is complex due to the coupling between the channels through pressure fields, but most importantly, because of the time-varying resistance as droplets are formed, enter, and exit channels.

$$\Delta P = RQ \tag{1}$$

where ΔP is the pressure drop $[Pa]$, R is the resistance across the channel $[Pa \cdot s/m^3]$, and Q is the flow rate $[m^3/s]$.

In addition to generally faster and more robust passive micro-channel networks, a better understanding of droplet resistance favours better droplet

trapping designs[8]. For example, immobilizing droplets enables the study of encapsulated cells over a period spanning hours of incubation[9, 10].

1.2 Literature overview

The current literature includes a variety of studies aiming to better understand how droplets affect flow in micro-channels. Although individual studies successfully demonstrate the validity of their data, a far-reaching consensus across the microfluidic community is still lacking. Hence, the design of complex passive microfluidic networks primarily relies on rules of thumb, iterative design, and previous experience; for example, the droplet length is estimated to increase the resistance 2 to 5 times more than it would be expected by an equivalent single-phase flow. Better droplet resistance quantification is envisioned to enable newcomers to the field to reach their final device design more quickly and more easily.

An overview of the various methods follows. Agreement and comparison between the various studies can be difficult due to the different approaches to droplet resistance quantification, range of Capillary number covered, dimensions, and flow-driving methods. Nonetheless, the approaches are separated into three broad categories: pressure sensors, loops, and interface comparison (flow-rate based). Numerical simulations and heat-transfer-oriented studies are omitted for the sake of conciseness but similarly to the studies herein included, the literature generally does not widely agree[11, 12].

1.2.1 Pressure sensors

The pressure tap method essentially uses pressure sensors to measure the pressure drop across a channel section containing one or more droplets. This approach is arguably the more intuitive and has been applied to both circular[13–16] and rectangular[17–22] cross-sections. Albeit the numerous studies, the variety of chip materials, geometry, continuous phase, and range of Capillary number make a consensus or even a comparison cumbersome. The studies involving circular capillaries appear to agree better with a $\pm$ $\sim$20% discrepancy with previous models[16]. There is nonetheless no clear agreement in the literature for the rectangular cross-section that is more typically used for complex microchannel networks made of polydimethylsiloxane (PDMS) devices for example. The flow physics differ between the circular and rectangular cross-section as a result of the complex gutter flow in the channel corners[23–25]. All these studies suffered from the same lack of pressure accuracy and time resolution arising inherently from the pressure tap approach. Thus, methods adopting an in-situ approach are deemed more promising.

1.2.2 Comparative loops

Observing the behaviour and traffic of droplets in a loop network minimizes the intrusiveness of the resistance measurement. The droplet resistance is derived from the comparison of the droplets in different sections of the network [26–29]

or in a different calibrated chip[30]. This method relies on assumptions about the flow and the uniformity of the droplets' resistance. Once again, the variety of channel dimensions, viscosity ratio, flow rate and even phase of the dispersed fluid (i.e. gas vs. liquid) makes an overarching relationship difficult to define. Another important factor is the presence and concentration of surfactants; their effects on flow are complex, but surfactants mainly impact surface tension, and hence the Capillary number. Moreover, the Marangoni stresses from the surfactant concentration gradient alters the flow[31]. Consequently, whether surfactant is present or not in either the dispersed or continuous phase hinders the comparison of the results of multiple studies.

1.2.3 Interface comparison

An interface between two fluids contrasted using a dye quantifies flow rate differences; the droplet resistance is determined based on the calibrated relationship between the interface displacement and corresponding excess flow rate[32, 33]. Thus, the interface essentially provides a localized flow sensor. Another similar method uses a small particle trapped using optical tweezers to quantify the changes in a channel adjacent to the one containing the droplet[34]. The following technique requires furthermore investigation to better assess the validity of the quantification of the droplet resistance. Nevertheless, the results using the resistance of single-phase flow through complex geometry are promising[35]. However, there is not a clear consensus with the results from other methods.

1.2.4 Detailed models

Another approach to understand droplet resistance relies on detailed theory-oriented models. Previous works include both rectangular[36, 37] and circular[38] cross-sections. However, the complexity of the equations prohibits a straightforward understanding of the factors determining droplet resistance. The complexity would only increase for additional consideration of factors such as cells or micro-particle concentration within the droplet and non-Newtonian behaviour of the fluids. These studies can nonetheless provide *qualitative* insights.

1.3 A novel approach using active control and system identification

A majority of the previous methods relied on a syringe pump to drive the flow. However, the persisting short-term and long-term oscillations of the syringe pump are well documented from previous studies[39]. In contrast, the present approach rather uses a pressure pump with fast response and better long term stability[40]. The quick pressure adjustment is a key consideration in the implementation of an active control platform[41, 42]. For this novel approach, the

ability of the active control platform to impose an individual droplet movement according to an arbitrary path is leveraged to apply system identification techniques.

2 Working principle

2.1 Active control of droplets using visual feedback

The active control platform uses a desktop computer to implement the controller and to establish communication with the different parts of the system. Figure 1 shows an overview of the flow of information for each sampling period of 100 ms. More details are included in previous work[41–43]. Essentially, an image analysis algorithm identifies the droplet location based on the interface between the two phases. This feedback is taken by the controller that then calculates the required pressure at each inlet of the microfluidic chip. The pressure pump provides quick actuation adjustments every sampling period.

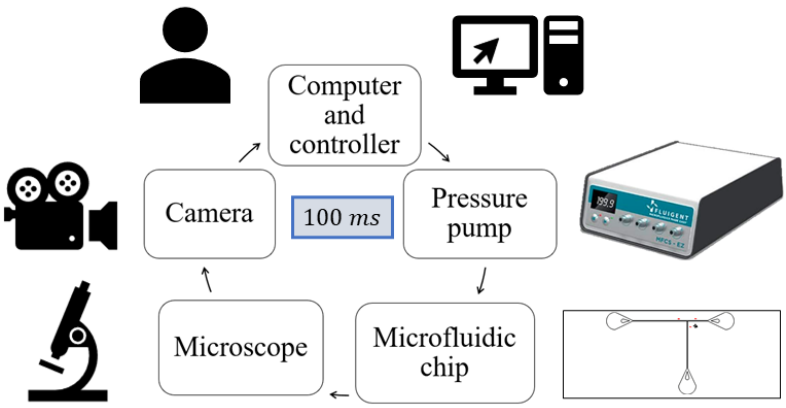

Fig. 1 Overview of the control loop implemented for the active platform (Fluigent MFCS-EZ pressure pump, Nikon Ti-E microscope, Andor Zyla sCMOS 5.5 camera).

2.2 System identification

The implementation of active control alone is not sufficient to provide further insight into droplet hydrodynamic resistance. However, its ability to make a droplet follow an arbitrary position reference signal is key to the application of system identification principles. The general workflow for system identification is shown in Figure 2. The first step is system actuation; the path the droplet follows is designed to enable the user to retrieve data providing information about the system. The input (applied pressures at the inlets) and output

(droplet position) data are simultaneously recorded as the active control operates. The *Matlab* `greyest` system identification algorithm generates a set of parameters including the resistance of the channel which contains the droplet that best fits the input-output data provided based on the imposed model structure. The droplet resistance is then retrieved from the channel resistance by subtracting the resistance contribution from the continuous phase.

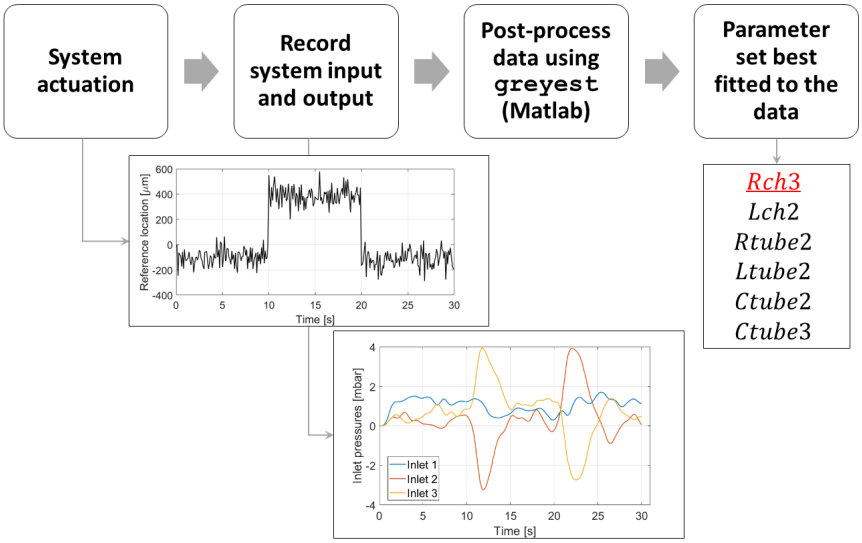

Fig. 2 A general workflow for system identification. (1) System actuation is necessary to excite the frequencies of interest. Without the proper choice of the arbitrary path to follow, the information provided by the system will not be informative enough (See Figure 4 for more details). (2) The input and output to the system (in this case, each inlet pressure and the droplet position) are simultaneously recorded while the system is actuated. (3) The recorded input-output data is post-processed using the Matlab `greyest` algorithm from the System Identification toolbox. (4) The system identification algorithm returns the set of parameters that best fit the input-output data provided. The parameter of interest is the resistance of channel 3 that contains a single droplet and is otherwise filled with the continuous phase. The subset of parameters is selected based on the identifiability analysis.

2.3 Identifiability analysis

For grey-box system identification, the number of parameters and model structure are rooted in physical principles expressed mathematically using differential equations. The identifiability analysis aims to decide whether the value of the parameters can be confidently determined from the input-output data or not. The overall identifiability property is a combination of the informativity of the experimental data and the identifiability of the model structure[44]. The mathematical definitions are of little insight here; hence, qualitative descriptions are included[45].

Experimental data informativity

The input-output data collected experimentally are informative if no other model could generate the same response.

Model structure identifiability

A model identifiability is resolved by the existence (or the lack thereof) of two different parameter sets describing the same system. Or more formally, the mapping from the parameter set to the model is injective.

2.3.1 Sensitivity

Varying an identifiable parameter value is expected to change both the state vector and outputs. The sensitivity quantifies the effects of varying a parameter; the normalized quantity is compared with the other model parameters in terms of order of magnitude. A relatively low sensitivity magnitude for a parameter indicates that it is harder to identify; changing its value does not affect as significantly the system behaviour compared to the other parameters values.

2.3.2 Collinearity of parameters

Highly collinear parameters compromise the model structure identifiability. Groups of collinear parameters can compensate for the change in one parameter by varying other parameters. Therefore, multiple sets of parameters yield the same response. Through the identifiability analysis, highly collinear parameters are determined and excluded from the subset of parameters to be identified.

The mathematical evaluation of the interplay between the different parameter subsets is implemented and automated in a Matlab-based toolbox [46]. The dependence between parameters is quantified using the collinearity index (CI). A low CI for a subset of parameters means they are *not* significantly collinear; thus, changes in one parameter cannot be compensated by other parameters within that subset. This ensures proper model structure identifiability. The CI quantification is based on the magnitude of the coefficients (α_i) required to make the following linear independence equation zero:

$$\sum_{i=1}^{k} \alpha_i \cdot \bar{s}_{K,i} = 0 \tag{2}$$

where K represents the k-th parameter subset composed of k parameters, α_i are the constants determining linear dependence if there exists a set of $\alpha_i \neq 0$ such that the above equation holds, and $\bar{s}_{K,i}$ is the normalized parameter sensitivity.

Correspondingly, the CI for the specific parameter subset K is defined as:

$$CI_K = \frac{1}{min_{\alpha=1}\bar{S}_K\alpha} \tag{3}$$

A group of parameters is deemed identifiable if the CI is less than 20 which corresponds to at least 95% compensation within the collinear parameter group for variations of the parameters outside of the group and at least 5% error for compensation of parameter change within the subset[47].

3 Experimental setup for droplet control

3.1 Materials and chip fabrication

The microfluidic chip is fabricated using a standard soft photo-lithography procedure[6]. Briefly, SU-8 photoresist is spin-coated on top of a silicon wafer. The micro-channel network is selectively exposed to UV light using a photo-mask. Afterwards, the unexposed SU-8 is washed away using photo-developer. The master is used to create a polydimethylsiloxane (PDMS, *Sylgard 184*) mould of the channel network that is then bonded to a glass slide covered with a thin layer of PDMS to ensure uniform surface property for droplet manipulation. The superhydrophobicity of the PDMS is retrieved through heating.

A PDMS chip is used to quantify droplet resistance as it is ubiquitous in the microfluidic community and is used in numerous studies. Furthermore, subtle effects such as the top wall deformation can have substantial importance due to the high power of the height parameter[48]. The difference between the nominal and the actual channel height is the product of multiple factors: variations in the thickness of the spin-coated SU-8 layer, variations in the mould height when transferred from the master, PDMS absorption causing swelling, and deformation from the applied pressure. These small but important circumstances are incorporated in this approach to closely mirror the usual setup with PDMS microfluidic chip applications.

3.2 Overview for experiment design

The continuous phase viscosity and channel length are considered to design an experiment favourable to identifying the changes from a single droplet contained in a microchannel. The channel resistance is considered as the sum of the length filled with the continuous phase and the dispersed phase droplet. The viscosity contrast between the dispersed and continuous phase influences the fluid flow profile within the channels. Typically, the continuous phase (such as silicone oil) is more viscous than the aqueous dispersed phase. Similarly to numerous other experiments previously summarized in Section 1.2, the viscosity ratio is selected fairly low ($2 < \mu_c/\mu_d < 5$). Hence, the changes from the

lower viscosity dispersed phase will more significantly affect the overall channel resistance. The selected dispersed phase is DI water while the continuous phase is silicone oil 5 cst.

Likewise, the channel length is selected as short as possible to maximize the influence of the droplet resistance on the overall channel resistance. Channel 3 contains the droplet and is 3 mm long. A shorter channel would increase too much the risk of the droplet overflowing either at the junction with the other channels or in the outlet. Channel 1 is connected to the dispersed phase reservoir and is 7 mm long. Channel 2 is connected to the continuous phase reservoir and is 8 mm long. The channel height and width are uniform for all channels at 40 µm and 100 µm respectively. The geometry is shown in Figure 3.

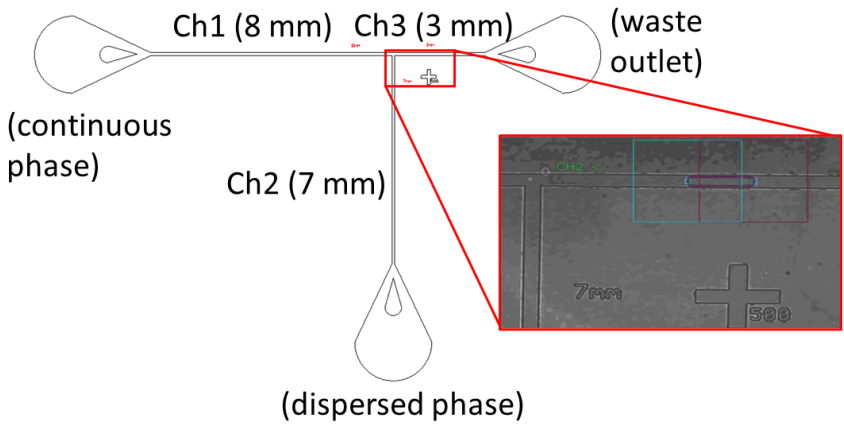

Fig. 3 2D geometry of the T-junction with a screen grab of a droplet in the channel 3. Supplementary material "S2 droplet requested position.gif" shows an example of droplet following the reference location.

3.3 Active control system implementation

3.3.1 System architecture

The active control platform enables the application of system identification methods to the quantification of droplet resistance; Figure 1 shows schematically its architecture. The equipment used is more specifically a Fluigent MFCS-EZ pressure pump that pushes the samples to the PDMS microfluidic chip. The Nikon Ti-E microscope with a 4X magnification objective is used to visualize the droplet in the micro-channel. The information is conveyed to the computer with the Andor Zyla sCMOS 5.5 camera. An image processing algorithm identifies the interface between the dispersed and continuous phases within the channel. The current position is passed on to the controller that

compares it against the desired position. The appropriate pressure for each chip inlet is then calculated and communicated to the pressure pump. The complete control loop executes every 100 ms, that is at 10 Hz.

The system architecture for droplet control serves two main purposes: droplet position control, and droplet generation. The feedback loop enables the trapping of droplets at a user-specified position [43]. Instead of using mouse movement, the software is updated to follow an arbitrary path from a file. The details are presented in the following subsection 3.3.2. The semi-automated control [42] generates droplets of a desired length. A single droplet can thus be generated and held in Channel 3 to assess its resistance.

3.3.2 Arbitrary requested position

The active control platform enables the user to select a droplet interface for which a pre-determined path is followed such as the one shown in Figure 4.

Implementation

A table containing the desired position at each millisecond is generated offline and loaded into the custom active control platform software. Each time the control loop executes, the elapsed time from the initial timestamp is used to look up in the table the current reference position. The controller calculates the appropriate pressure to apply to each inlet and these are then communicated to the pressure pump.

Design justification

The reference position that the droplet is following must provide informative experimental data. A single sinusoidal input would allow identifying a couple of parameters[49]. The informativity of the input-output data is ensured by providing a complex reference signal that excites numerous frequencies using white noise. However, the arbitrary reference position signal is not the input data required by the system identification algorithm. The pressure input is determined by the controller based on the reference signal and the current droplet position. Hence, the frequency content of the input provided to the system identification algorithm is filtered from the arbitrary path based on the sampling rate of 10 Hz of the controller. This limits the excitability of the signal; however, extensive modifications to the active control platform are required to accommodate a faster sampling rate.

The sampling rate is limited by the architecture and hence a time-response approach is selected over the frequency-domain approach. However, simple step responses do not provide enough information about the system. Thus, white noise is added to better excite the system. Furthermore, although the active droplet control system enables the user to specify an arbitrary path for the droplet to follow within a channel, the model is based on droplet velocity. The white noise is added to a up-and-down step to capture the hysteresis effects and average the behaviour over both cases. The 500 μm step allows the droplet to reach a greater velocity than with a pseudorandom binary sequence (PBS).

Droplet behaviour in micro-channels depends on the droplet velocity generally expressed using the Capillary number. From the peak velocity, the Capillary number for all experiments is less than 10^{-3}.

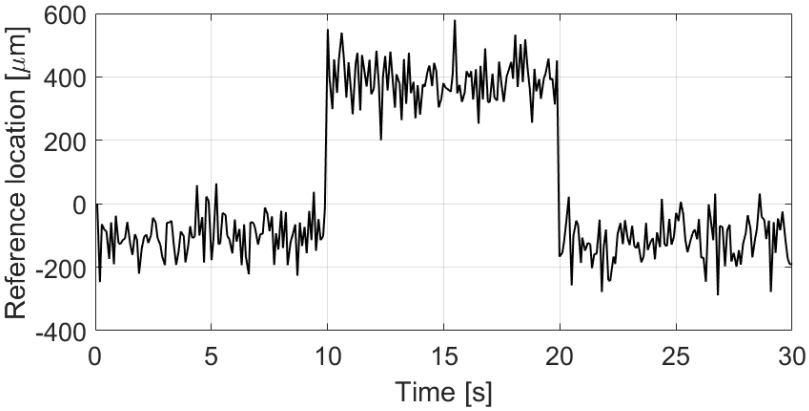

Fig. 4 Arbitrary reference position signal for the droplet interface in the channel of interest (Ch3). Supplementary material "S2 droplet requested position.gif" shows an example of droplet following the reference location.

4 System identification methodology

The *Matlab* System Identification toolbox is leveraged with its grey-box system identification algorithm. The `greyest` function from the toolbox developed by L. Ljung is used as-is. The set of parameters to identify are selected based on the identifiability analysis.

4.1 Data separation

Three different sets of experiments are carried out for each droplet-length-to-channel-width ratio with at least two different chips on two different days. Each set of experiments is composed of 10 steps up and down (as shown in Figure 4) that are subsequently separated into 30-second intervals for each of the 10 datasets.

4.2 Data pre-filtering

To avoid fitting the parameters to noise, both the input and output data are pre-filtered to reject high-frequency noise. Hence, the analysis concentrates on the frequencies of interest of the model. Briefly, the zero-phase delay filter (`filtfilt`) function from Matlab is used with a low-pass filter frequency of 10 Hz. This ensures no shift or delay.

4.3 `greyest` algorithm

The built-in System Identification Matlab toolbox is used. Grey-box system identification is used rather than a black-box approach to retain the physical meaning of the identified model parameters. The resources for grey-box system identification are somewhat limited, especially when considering a multi-input multi-output (MIMO) system. The user-defined model is in the state-space format. The algorithm finds the set of parameters that best fits the provided input-output data.

4.3.1 State-space model structure

The model developed is based on the physical parameters of the system. In this case, these parameters include the channel dimensions, the fluid viscosity, etc. The physical properties are translated to RLC circuit elements similar to the previous design strategy[41]. Differently, the sub-block circuit is a symmetric circuit with the resistance and the inductance equally distributed on either side of the capacitance. Moreover, using *Simulink* to easily obtain the state-space matrices with the *numerical* values is irrelevant; the system equations must be derived analytically to retrieve them in their symbolic form.

The lengthy and cumbersome resulting matrices are included in ESI.S1[†]. The general expression and nomenclature are nevertheless outlined below. This model only encapsulated the physics of the fluid tubing from the reservoir holder to the microfluidic chip and the chip itself; hence the "tc" subscript used.

$$\dot{x}_{tc} = A_{tc} \cdot x_{tc} + B_{tc} \cdot u_{tc} \tag{4}$$

$$y = C_{tc} \cdot x_{tc} + D_{tc} \cdot u_{tc} \tag{5}$$

where x_{tc} is the state vector composed of currents and potentials, A_{tc} is the state transition matrix and is a function of all the parameters $(RchX, LchX, CchX, RtubeX, LtubeX, CtubeX)$, B_{tc} is the input matrix and is a function of $LtubeX$ only, u_{tc} is the input pressure at each fluid tubing inlet $(P1,\ P2,\ P3)$ in the reservoir holder, y is the output vector for the droplet *velocity*, C_{tc} and D_{tc} are the output equation matrices.

4.3.2 Tubing dynamics

The pump software provides the pressure measurement at each of its outlets. However, the pressure at the pump output does not instantaneously and exactly correspond to the pressure at the fluid tubing inlet $(P1, P2, P3)$. The soft air tubing connecting each pump output to the reservoir holder introduces dynamics of its own that are previously investigated[50]. For the air tubing used (1X3 mm diameter and 66.5 cm length), the first-order model (G_{air}) has a scaling constant (k) of 1 and time constant (τ) of 33 ms. The scaling constant is simply one because any static offset is estimated using a Kalman Filter

and compensated in the input data.

$$G_{air}(s) = \frac{u_{tc}}{u_{pump}} = \frac{1}{0.033 \cdot s + 1} \tag{6}$$

The combination of the air tubing dynamics with the fluid tubing and chip dynamics is straightforwardly implemented using matrix concatenation.

$$\dot{X} = \begin{bmatrix} \dot{x}_{tc} \\ \dot{u}_{tc} \end{bmatrix} = \begin{bmatrix} A_{tc} & B_{tc} \\ 0 & -1/\tau \end{bmatrix} \cdot \begin{bmatrix} x_{tc} \\ u_{tc} \end{bmatrix} + \begin{bmatrix} 0 \\ k/\tau \end{bmatrix} \cdot u_{pump} \tag{7}$$

$$y = \begin{bmatrix} C_{tc} & D_{tc} \end{bmatrix} \cdot \begin{bmatrix} x_{tc} \\ u_{tc} \end{bmatrix} + \begin{bmatrix} 0 \end{bmatrix} \cdot u_{pump} \tag{8}$$

4.4 Parameter subset used for identification

The number of parameters of a model describing a system is a trade-off between the fit to a specific dataset used for identification purposes and the prediction error with another dataset obtained from the same system. Figure 5 conceptually represents the trade-off. Ideally, the model is complex enough to capture the dynamics of the system while retaining a low model prediction error. A validation data set verifies for over-parametrization.

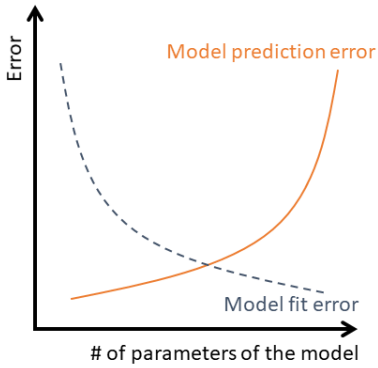

Fig. 5 Relationship between the number of parameters and the fit to a single input-output data set. Over-parametrization lead to poor fit to other datasets from the same system. A validation data set is used to verify adequate fit to another input-output dataset.

In addition to the number of parameters, the specific subset of parameters to include must be selected. The state-space model of the T junction considers the tubing and channels for the 3 branches and comprises 18 parameters (see Supplementary material "S1 State-space model structure" for the model

details). A resistance, an inductance, and a capacitance are associated with each tubing and microchannel. The first letter of the parameter indicates its type: "R" for resistance, "L" for inductance, and "C" for capacitance. The second part specifies whether the component is for the channel ("ch") or the tubing from the reservoir holder to the microfluidic chip ("tube"). Finally, the number indicates the branch of the T-junction (see Figure 3).

However, as outlined in Section 2.3, the mathematical formulation of the model impacts the efficacy of the grey-box system identification algorithm. If subgroups of highly collinear parameters are included in the identification scheme, then different sets of parameters can result in the same output. The compromised model structure identifiability means that changes in one parameter can be compensated by changes in other parameters. Therefore, the parameters included must be carefully selected to provide informative results; the excluded parameters are fixed to their nominal values used for controller design.

The analysis of the numerous parameters would be too cumbersome to complete manually. Hence, a more automated and numerical approach for the identifiability analysis is implemented using a Matlab-based toolbox developed by Gabor *et al.*[46]. There are four components summarized in Figure 6: (a) parameter sensitivity, (b) largest identifiable subgroup, (c) highly collinear parameters, and finally, (d) the identifiable parameters. The key parameter that must be identifiable is Rch3 because this channel contains the single droplet.

(a) Parameter sensitivity

The influence of each parameter on the states and the outputs is quantified with a normalized magnitude. The parameters that have an influence several orders of magnitude lower than the maximum magnitude are disregarded as they are not identifiable. Their small influence on the output potentially indicates a model over-parametrization. Nevertheless, eliminating parameters requires the resulting model to also exhibit the desired identifiability behaviour. Hence, although different models are assessed, only the full model with the 18 parameters and the tubing dynamics yields satisfactory results as will be demonstrated. The parameter of interest (i.e. Rch3) must have a sensitivity of the same order of magnitude as the maximum one to be potentially identifiable, as shown in Figure 6(a).

(b) Largest identifiable subgroup size

The sensitivity analysis eliminates parameters that are more problematic to quantify. Nonetheless, *all* of the other parameters are not necessarily identifiable. Due to the potential collinearity between parameters, a smaller identifiable subset must be determined. A combinatorial optimization approach is implemented in the toolbox[46] to find the largest group possible for the collinearity index threshold. A threshold of 20 is deemed satisfactory as it means that: (i) variations in the parameters *outside* of the subgroup can be

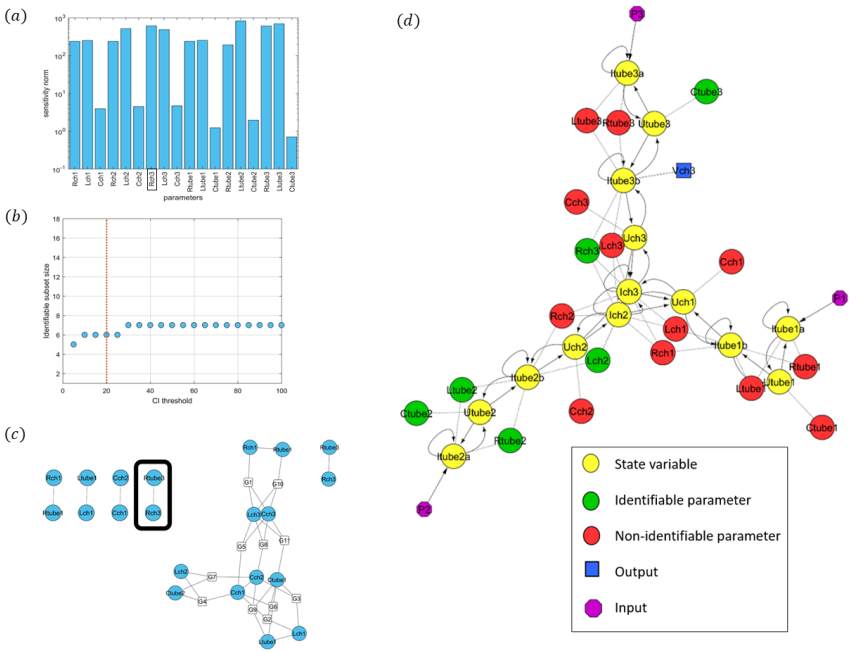

Fig. 6 Identifiability analysis of the RLC state-space model with 18 parameters. (a) parameter sensitivity: Rch3 (black box) has a comparable sensitivity norm to 11 other parameters. (b) largest identifiable subgroup: only subgroups of up to 8 parameters are identifiable based on collinearity. (c) highly collinear parameter groups: the selected subgroup has a high collinearity between Rch3 and Rtube3 only. (d) identifiable parameters : Bond-like graph of the selected subgroup of parameters.

compensated at least to 95%, and (ii) variations to a parameter *within* the subgroup is associated with an error of at least 5% when compensated for.

Multiple subgroups satisfy the collinearity index of 20 with the largest including 6 parameters. The appropriate subgroup K must include the targeted parameter (i.e. Rch3). Furthermore, the analysis of the highly collinear parameter groups must isolate the parameter of interest within a small group. The values of these highly collinear parameters must be reasonably known as further detailed in part (c).

(c) Groups of highly collinear parameters

The collinearity between the parameters within the selected subgroup K is further analyzed using its quantification through the collinearity index (CI_K). Highly collinear parameters are grouped together. These subgroups indicate that any inaccuracy in the nominal values of the non-identifiable parameters will be reflected in the value of the identifiable parameter from the subgroup.

Ideally, the parameter of interest–Rch3–would be isolated and have a low collinearity index with all other parameters. However, the structure of the

model and the output information available imposes the collinear group relationships. The discrepancy between the nominal values of the parameters excluded from the subgroup will be reflected in the identified values of the other parameters. The best-case scenario, as shown in Figure 6(c), is the grouping between Rtube3 and Rch3 only. Thus, any inaccuracy in the nominal value of Rtube3 will be reflected in the identified value of Rch3; however, the value of Rtube3 is experimentally determined with confidence from a separate set of data using a flow sensor. Only Rch3 amongst the identifiable parameters is confidently identified as concluded by this analysis. Nevertheless, Rch3 is the only parameter required to quantify the droplet resistance.

(d) Identifiable parameters

The result of the identifiability analysis is visualized graphically in Figure 6(d) similarly to a Bond graph. The identifiable parameters are indicated with green circles. The six parameters that are identifiable as concluded by this identifiability analysis are: Rch3, Lch2, Rtube2, Ltube2, Ctube2, and Ctube3. However, as previously mentioned, the uncertainty in the other parameters–except for Rtube3 that is confidently experimentally determined–means that only Rch3 is accurately quantified.

4.5 Parameter set validation

Given one set of input-output data, the fit can be arbitrarily increased by increasing the number of parameters. However, then, the prediction error for an independent input-output dataset increases from over-parametrization as illustrated conceptually in Figure 5. Therefore, the model complexity–quantified using the number of parameters–is a trade-off between the fit to the dataset used to determine the parameter, and the model prediction error of an independent dataset. Moreover, the complexity of the identifiability analysis increases with the number of parameters. The mathematical principles are implemented through *Matlab* toolboxes (i.e. *AMIGO2* and *VisID*[46]) to avoid the overly complex analytical approach. A straightforward validation of a particular set of parameters is used to simulate the system with another set of input data: the validation data. Then, the measured output is compared with the simulated output to verify that the fit is reasonable. A much lower fit with the validation dataset indicates over-parameterization.

4.6 How to calculate droplet resistance from the total channel resistance

The grey-box system identification algorithm determines the set of parameters that best fits the data based on the specified model structure. The parameter of interest within the set is the resistance of the channel containing the droplet that is moved according to the designed path (Rch3). The length of the droplet is varied in different sets of experiments, but the channel length is kept constant.

The resistance of single-phase flow is well established compared to the resistance of two-phase flow (*i.e.* droplet resistance). As per the Hagen-Poiseuille law (Equation 1), the dimensions are used to calculate the channel resistance for single-phase flow. Equation 9 is for the resistance of a channel for which the height is at least half of the width [7].

$$R_{rectangle} = \frac{12\eta L}{1 - 0.63(h/w)} \frac{1}{h^3 w} \tag{9}$$

where R is the resistance $[Pa \cdot s/m^3]$, η is the dynamic viscosity $[Pa \cdot s]$, L is the channel length $[m]$, h is the channel height $[m]$ and w is the channel width $[m]$.

According to the model structure imposed through the grey-box system identification (see Section 4.3), the resistance determined experimentally is for the full channel ($R_{channel}$ as per Figure 7). The channel length is maintained constant for all experiments for simplicity. Therefore, in order to calculate the droplet resistance ($R_{droplet}$) from the resistance given by the grey-box system identification algorithm ($Rch3$), the resistance contributed by the continuous phase ($R_{continous}$) must be compensated for using single-phase theory (Equation 9) as shown in Equation 10.

$$R_{droplet} = R_{channel} - R_{continuous} \tag{10}$$

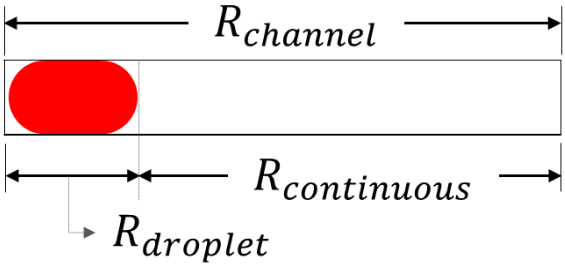

Fig. 7 Schematic representation of the total channel resistance ($R_{channel}$) as the sum of the droplet resistance ($R_{droplet}$) and the rest of the channel filled with the continuous phase ($R_{continuous}$).

4.7 Resistance ratio

The experimental droplet resistance calculated as per Section 4.6 is compared to the equivalent single-phase resistance. The ratio quantifies how much additional resistance the droplet is causing. This additional resistance is attributed to the Laplace pressure from the asymmetric leading and trailing caps, the gutter flow, and the thin film flow. The droplet resistance ratio (DRR) is the

quotient of experimental to single-phase resistance; this is the ratio informally estimated as 2 to 5 for passive channel network design.

$$DRR = \frac{R_{droplet,exp}\ (Eq.\ 10)}{R_{droplet,single-phase}\ (Eq.\ 9)} \tag{11}$$

4.8 Statistical significance of the results

The impact of the droplet on the overall channel resistance are expected to be small even with the intentional design as per Section 3.2. The challenging quantification partly explains the difficult agreement between the studies summarized in the literature overview.

Graphical representation of the data spread using error bars with their magnitude equal to one standard deviation is deemed inappropriate because of their closeness. Consequently, the statistical significance of the resistance compared to other droplet length ratios is rather determined using a statistic test on the difference of means. The 95% confidence interval of the mean difference is calculated based on the unknown population variances[51]. If the interval includes zero, then, it is concluded that there is no statistically significant difference between the two sample means.

$$\Delta\bar{x} - t_{\alpha/2,\nu}\sqrt{\frac{s_1^2}{n_1} + \frac{s_2^2}{n_2}} \leq \Delta\mu \leq \Delta\bar{x} + t_{\alpha/2,\nu}\sqrt{\frac{s_1^2}{n_1} + \frac{s_2^2}{n_2}} \tag{12}$$

where $\Delta\bar{x}$ is the difference in *sample* means, $t_{\alpha/2,\nu}$ is taken from the Student's t distribution with $\alpha = 0.05$ for the 95% confidence interval and ν is the degree of freedom calculated using Equation 13 rounded down to the nearest integer, s_1 and s_2 are the standard deviation of the first and second sample respectively, n_1 and n_2 are the number of data points for each sample, and $\Delta\mu$ is the difference in mean of the *population*.

$$\nu = \frac{(s_1^2/n_1 + s_2^2/n_2)^2}{\frac{(s_1^2/n_1)^2}{n_1-1} + \frac{(s_2^2/n_2)^2}{n_2-1}} \tag{13}$$

5 Results and discussion

5.1 Experimental droplet hydrodynamic resistance

The fit of the nominal set of parameters is graphically compared to one of the identified sets of parameters in Figure 8. The actual system output shown in grey is the target that the system identification algorithm tries to match by considering the input data and varying the parameters. Fit improvement is observed. The dashed red rectangle shows a region of fast oscillations that are faster than any expected response of the system. Thus, this region indicates an over-parametrization of the model. Nevertheless, the identifiability analysis is suitable to quantify Rch3 using this model structure. By changing the model

structure and reducing the number of parameters, a new identifiability analysis yielding similar results would be required and could not be achieved. Hence, the RLC model is retained.

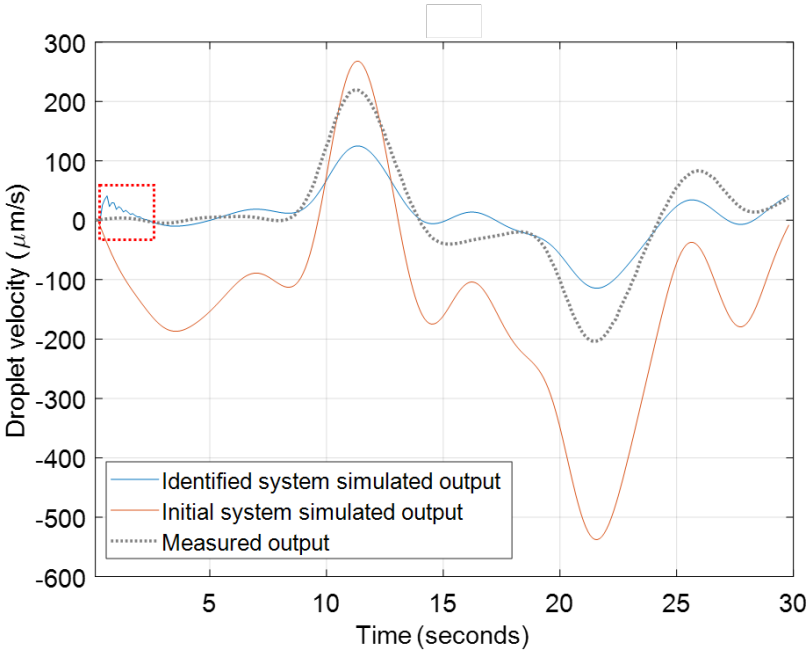

Fig. 8 Model simulation of nominal and identified model compared to the actual recorded system output. The identified output (blue) is the simulation results from the identified parameters. The initial system output (orange) is the simulation results from the nominal parameters (values from previous work). The measured output (dotted black) is the actual measured output of the droplet velocity. The dashed red rectangle shows oscillations too fast for the physical system indicating potential over-parametrization.

The model fit for each identified set of parameters is plotted in Figure 9 against the corresponding Rch3 resistance. The system identification algorithm essentially optimizes the value of the parameters to minimize the discrepancy between the measured and simulated system output. The identifiability analysis aims to select a parameter subgroup that effectively reduces the equivalent local minima that would lead to the algorithm converging to different sets of parameters with the same response. Although the selected set of six parameters reduces the spread of the identified value for Rch3, there is still a considerable range of values. Therefore, the results are selected based on a threshold of 50% model fit for the simulated system compared with the actual system. Figure 9 shows that the values for Rch3 are grouped closer at higher percent fit.

The selected data points based on model fit are shown in Figure 10(a). The values of the resistance of the channel containing the droplet (Rch3) have a relatively large standard deviation. This is further discussed in Section 5.3.

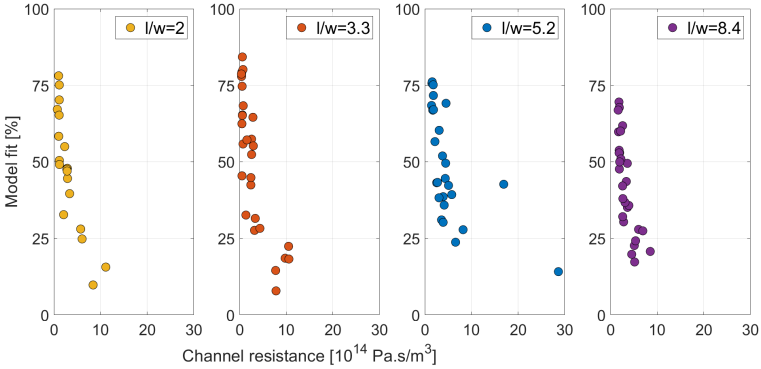

Fig. 9 A set of identified parameters is associated with each measurement dataset. All identified values of the parameter of interest (Rch3) are compared using the model fit. A higher model fit indicates a better match between the measured and simulated output using the identified parameter values. Only values of Rch3 corresponding to a 50% model fit or higher are considered henceforth. The model fit value is defined as per the Matlab `compare` function ($100\left(1-\frac{|y-\hat{y}|)}{|y-mean(y)|}\right)$).

The experimental droplet resistance and ratio are calculated as per Equations 10 and 11 respectively (see Figure 10(b)). The error bars are omitted due to their closeness. Instead, a statistical test on the mean is used to determine which data points are statistically significant from the others.

The statistical analysis demonstrates that some points are statistically insignificant from each other. Hence, the method herein presented does not have the resolution to distinguish between the two smaller and the two larger length-to-width ratios. The inclusion of the tubing dynamics is key to obtaining statistically meaningful results and supports the significance of this often, if not always, overlooked part of the microfluidic system [50].

5.2 Comparison with literature results

The numerous studies in the literature cover a wide range of parameters with varying chip material, cross-section dimensions and shape, viscosity contrast, surfactant used, Capillary numbers and many more. Nonetheless, a qualitative comparison between the results from Figure 10 is useful to assess the validity of this novel approach to droplet resistance quantification that leverages active droplet control.

The general trend of the additional resistance from the droplet is a sharp increase from small to medium length-to-width ratios, after which a steady linear decrease is observed for larger ratios. The sharp increase in the peak resistance ratio is higher for smaller Capillary numbers and lower dispersed to continuous phase viscosity contrast[32]. For a viscosity contrast around 0.2 and a Capillary number less than 10^{-3}, the peak resistance ratio is around 3.5 that is significantly lower than the 6.5 herein quantified[30]. However, the Capillary number is based on the maximum droplet velocity that is only achieved

at the step increase and decrease which can potentially contribute to this discrepancy. Nevertheless, the reasonable agreement with the previous literature consolidates this initial investigation that leverages the active droplet control platform to apply system identification techniques to quantify droplet resistance.

5.3 Limitations

5.3.1 System hardware

The resolution of the droplet resistance ratio is limited as shown in Figure 10(b). The results are nonetheless promising for the further development of the technique to improve the resolution. The technique could be applied more readily than the other approaches to a wide variety of channel geometries and fluid used, even potentially non-Newtonian fluids that still require fundamental research to better understand them. A better resolution is however necessary.

The control sampling rate of 10 Hz (i.e. at 100 ms intervals) limits the frequency content of the input and output data. Although a fast pressure measurement apparatus was developed to quantify the impact of the air tubing connecting the pump output to the reservoir holder (*i.e.* the input), the image processing (*i.e.* the output) is the limiting factor here. Significantly improving the image processing to identify the droplet location is outside the scope of the current work but is envisioned for the future. Moreover, the pressure measurement apparatus would also be required to be further developed to enable three independent pressure sensors, one for each branch of the T junction.

The compounding effects of the sampling frequency and the droplet position to calculate the droplet velocity are not fully analyzed. The velocity must be used as the output rather than the position; the plant to be identified must be strictly stable for the system identification algorithm.

5.3.2 Experiment parameters

The experimental results are limited by the parameter values investigated. The viscosity ratio (μ_c/μ_d) is about 5. The droplet length to width is varied from 2 to 8.5. All micro-channels have a height of about 40 µm. The maximum pressure differential is about 5 mbar in order for the droplet to follow the reference position. The equilibrium pressure is about 200 mbar.

The Capillary number varies with the back-and-forth of the droplet. The Capillary number is generally bounded by an upper value ($Ca < 10^{-3}$). The varying Capillary number value and the discrepancy with other experimental parameters hinder the quantitative comparison with results from the literature. Furthermore, the droplet resistance is expected to vary with the Capillary number. Therefore, the droplet resistance data herein presented is averaged over a time-varying low Capillary number.

The droplet velocity is measured using image processing to track and record the interface position. The model state variable is the flow rate within the channel. Therefore, uncertainties are introduced because of the velocity discrepancy

between the continuous phase and the droplet. Nevertheless, the velocity discrepancy is expected to be less than 5 % for a viscosity ratio of about 0.2 and length-to-width ratios between 2 and 8.5[24].

6 Conclusion

6.1 Summary

Quantifying droplet resistance has attracted research efforts from various angles including pressure taps and interface comparison to quantify flow rate. However, the body of research covers a wide range of conditions. Although each study agrees and draws conclusions in accordance with their data, a consensus has yet to be reached due to the complexity of the phenomenon. The active droplet control platform offers a novel and distinctive approach that uses system identification methods.

The active control enables the user to set an arbitrary path for the droplet. As the droplet moves back and forth following a step with added white noise, the input (i.e. pressure) and output (i.e. droplet position) are recorded. Matlab offers a pre-packaged grey-box identification algorithm that can post-process the input-output data. The model structure is fixed to retain the physical meaning of the parameters. The subset of parameters to identify is carefully selected based on the identifiability analysis to ensure their accuracy and narrower distribution. The system identification algorithm optimizes the parameter value to minimize the difference between the recorded system output and the simulated system output based on the recorded input. The subset of parameters includes the resistance of the channel containing the single droplet. From the known channel length and tubing resistance, the ratio of the experimental droplet resistance to the equivalent single-phase resistance is calculated.

Due to the current limitations of the approach, the resolution of the identified droplet resistance ratio identifies only two levels although four droplet length to channel ratio were tested. Nevertheless, the overall trend is in agreement with previous literature results. A sharp increase in resistance ratio is expected before a steady decrease; the steady decrease region is omitted because of our method's limitation of the droplet length. This proof of concept aligns with the literature but could be further developed to increase its impact and test numerous other conditions.

6.2 Future work

The scope of this paper is to present and verify the novel approach to quantify hydrodynamic droplet resistance using active control and system identification. Although the droplet resistance ratio obtained offers a crude resolution, the results are in agreement with previous literature. This is promising as key improvements to this approach could enable droplet resistance ratio quantification for a wide variety of conditions, chip geometry and even non-Newtonian

fluids. There are three main approaches to obtain better resolution for the droplet resistance ratio: upgraded active control platform, targeted system design, and improved identifiability and system identification analysis.

An upgraded active control platform could provide better (i.e. more accurate, more frequent) input-output data. Moreover, additional measurements such as flow rate of the tubing could better quantify Rtube3 and also help the system identification analysis to compensate for the leaking of the continuous phase through the gutter and thin film flow.

The identifiability analysis is typically applied to an unknown fixed system for which certain parameters must be quantified. However, in this study, there is some leniency in terms of chip design that could be better informed through an in-depth identifiability analysis. This could help the system identification algorithm converge more consistently to the same minima and narrow the data spread.

The grey-box algorithm used is from the Matlab system identification toolbox while the identifiability analysis is performed separately by a toolbox developed by another research group. A better synergy between the identifiability and identification algorithm could enable more reliable convergence to solutions and narrower parameter value spread.

With these improvements and the consequent better quantification resolution, a more thorough study could consider a lot more parameters such as viscosity ratio, channel aspect ratio, a wider variation of droplet length to channel width ratio, different materials, and most importantly, non-Newtonian fluids.

Acknowledgements

Marie would like to acknowledge the help of Attila Gabor in setting up the AMIGO2 [https://sites.google.com/site/amigo2toolbox/] and VisID [https://github.com/gabora/visid] Matlab toolboxes for the identifiability analysis[46].

Conflict of interest

All authors declare that they have no conflicts of interest.

Data availability statement

All data that support the findings of this study are included within the article (and any supplementary files).

References

[1] Patinglag, L., Sawtell, D., Iles, A., Melling, L.M., Shaw, K.J.: A microfluidic atmospheric-pressure plasma reactor for water treatment. Plasma Chemistry and Plasma Processing, 1–15 (2019)

[2] Cao, H., Zhou, X., Zeng, Y.: Microfluidic exponential rolling circle amplification for sensitive microrna detection directly from biological samples. Sensors and Actuators B: Chemical **279**, 447–457 (2019)

[3] Luo, G., Du, L., Wang, Y., Wang, K.: Recent developments in microfluidic device-based preparation, functionalization, and manipulation of nano- and micro-materials. Particuology (2019)

[4] Anna, S.L.: Droplets and bubbles in microfluidic devices. Annual Review of Fluid Mechanics **48**(1), 285–309 (2016). https://doi.org/10.1146/annurev-fluid-122414-034425

[5] Chen, X., Ren, C.L.: A microfluidic chip integrated with droplet generation, pairing, trapping, merging, mixing and releasing. RSC Advances **7**(27), 16738–16750 (2017)

[6] Qin, D., Xia, Y., Whitesides, G.M.: Soft lithography for micro-and nanoscale patterning. Nature protocols **5**(3), 491 (2010)

[7] Bruus, H.: Theoretical Microfluidics vol. 18. Oxford university press Oxford, ??? (2008)

[8] Bithi, S.S., Nekouei, M., Vanapalli, S.A.: Bistability in the hydrodynamic resistance of a drop trapped at a microcavity junction. Microfluidics and Nanofluidics **21**(11), 164 (2017)

[9] Huebner, A., Bratton, D., Whyte, G., Yang, M., Demello, A.J., Abell, C., Hollfelder, F.: Static microdroplet arrays: a microfluidic device for droplet trapping, incubation and release for enzymatic and cell-based assays. Lab on a Chip **9**(5), 692–698 (2009)

[10] Bai, Y., Patil, S., Bowden, S., Poulter, S., Pan, J., Salmond, G., Welch, M., Huck, W., Abell, C.: Intra-species bacterial quorum sensing studied at single cell level in a double droplet trapping system. International journal of molecular sciences **14**(5), 10570–10581 (2013)

[11] Talimi, V., Muzychka, Y., Kocabiyik, S.: A review on numerical studies of slug flow hydrodynamics and heat transfer in microtubes and microchannels. International Journal of Multiphase Flow **39**, 88–104 (2012)

[12] Abdollahi, A., Sharma, R.N., Vatani, A.: Fluid flow and heat transfer of liquid-liquid two phase flow in microchannels: A review. International Communications in Heat and Mass Transfer **84**, 66–74 (2017)

[13] Kashid, M.N., Agar, D.W.: Hydrodynamics of liquid–liquid slug flow capillary microreactor: flow regimes, slug size and pressure drop. Chemical

Engineering Journal **131**(1-3), 1–13 (2007)

[14] Jovanović, J., Zhou, W., Rebrov, E.V., Nijhuis, T., Hessel, V., Schouten, J.C.: Liquid–liquid slug flow: hydrodynamics and pressure drop. Chemical Engineering Science **66**(1), 42–54 (2011)

[15] Xu, K., Tostado, C.P., Xu, J.-H., Lu, Y.-C., Luo, G.-S.: Direct measurement of the differential pressure during drop formation in a co-flow microfluidic device. Lab on a Chip **14**(7), 1357–1366 (2014)

[16] Ładosz, A., Rigger, E., von Rohr, P.R.: Pressure drop of three-phase liquid–liquid–gas slug flow in round microchannels. Microfluidics and Nanofluidics **20**(3), 49 (2016)

[17] Cubaud, T., Ho, C.-M.: Transport of bubbles in square microchannels. Physics of fluids **16**(12), 4575–4585 (2004)

[18] Adzima, B.J., Velankar, S.S.: Pressure drops for droplet flows in microfluidic channels. Journal of Micromechanics and Microengineering **16**(8), 1504 (2006)

[19] Salim, A., Fourar, M., Pironon, J., Sausse, J.: Oil–water two-phase flow in microchannels: Flow patterns and pressure drop measurements. The Canadian Journal of Chemical Engineering **86**(6), 978–988 (2008)

[20] Cybulski, O., Garstecki, P.: Transport of resistance through a long microfluidic channel. Physical Review E **82**(5), 056301 (2010)

[21] Kim, N., Murphy, M.C., Soper, S.A., Nikitopoulos, D.E.: Liquid–liquid segmented flows in polycarbonate microchannels with cross-sectional expansions. International Journal of Multiphase Flow **58**, 83–96 (2014)

[22] Ładosz, A., von Rohr, P.R.: Pressure drop of two-phase liquid-liquid slug flow in square microchannels. Chemical Engineering Science **191**, 398–409 (2018)

[23] Baroud, C.N., Gallaire, F., Dangla, R.: Dynamics of microfluidic droplets. Lab on a Chip **10**(16), 2032–2045 (2010)

[24] Jakiela, S., Makulska, S., Korczyk, P.M., Garstecki, P.: Speed of flow of individual droplets in microfluidic channels as a function of the capillary number, volume of droplets and contrast of viscosities. Lab on a Chip **11**(21), 3603–3608 (2011)

[25] Korczyk, P.M., van Steijn, V., Blonski, S., Zaremba, D., Beattie, D.A., Garstecki, P.: Accounting for corner flow unifies the understanding of droplet formation in microfluidic channels. Nature communications **10**(1),

2528 (2019)

[26] Fuerstman, M.J., Lai, A., Thurlow, M.E., Shevkoplyas, S.S., Stone, H.A., Whitesides, G.M.: The pressure drop along rectangular microchannels containing bubbles. Lab on a Chip **7**(11), 1479–1489 (2007)

[27] Schindler, M., Ajdari, A.: Droplet traffic in microfluidic networks: A simple model for understanding and designing. Physical Review Letters **100**(4), 044501 (2008)

[28] Labrot, V., Schindler, M., Guillot, P., Colin, A., Joanicot, M.: Extracting the hydrodynamic resistance of droplets from their behavior in microchannel networks. Biomicrofluidics **3**(1), 012804 (2009)

[29] Sessoms, D., Belloul, M., Engl, W., Roche, M., Courbin, L., Panizza, P.: Droplet motion in microfluidic networks: Hydrodynamic interactions and pressure-drop measurements. Physical Review E **80**(1), 016317 (2009)

[30] Jakiela, S.: Measurement of the hydrodynamic resistance of microdroplets. Lab on a Chip **16**(19), 3695–3699 (2016)

[31] Luo, Z.Y., Shang, X.L., Bai, B.F.: Marangoni effect on the motion of a droplet covered with insoluble surfactant in a square microchannel. Physics of Fluids **30**(7), 077101 (2018)

[32] Vanapalli, S.A., Banpurkar, A.G., van den Ende, D., Duits, M.H., Mugele, F.: Hydrodynamic resistance of single confined moving drops in rectangular microchannels. Lab on a Chip **9**(7), 982–990 (2009)

[33] Choi, S., Lee, M.G., Park, J.-K.: Microfluidic parallel circuit for measurement of hydraulic resistance. Biomicrofluidics **4**(3), 034110 (2010)

[34] Jin, Y., Orth, A., Schonbrun, E., Crozier, K.B.: Measuring the pressures across microfluidic droplets with an optical tweezer. Optics express **20**(22), 24450–24464 (2012)

[35] Suteria, N.S., Nekouei, M., Vanapalli, S.A.: Microfluidic bypass manometry: highly parallelized measurement of flow resistance of complex channel geometries and trapped droplets. Lab on a Chip **18**(2), 343–355 (2018)

[36] Wong, H., Radke, C., Morris, S.: The motion of long bubbles in polygonal capillaries. part 1. thin films. Journal of Fluid Mechanics **292**, 71–94 (1995)

[37] Rao, S.S., Wong, H.: The motion of long drops in rectangular microchannels at low capillary numbers. Journal of Fluid Mechanics **852**, 60–104 (2018)

[38] Hodges, S., Jensen, O., Rallison, J.: The motion of a viscous drop through a cylindrical tube. Journal of fluid mechanics **501**, 279–301 (2004)

[39] Korczyk, P.M., Cybulski, O., Makulska, S., Garstecki, P.: Effects of unsteadiness of the rates of flow on the dynamics of formation of droplets in microfluidic systems. Lab on a Chip **11**(1), 173–175 (2011). 10.1039/c0lc00088d

[40] Kieffer, C.-A., Ritty, S., Boudot, T., Petit, N., Weber, J., Le Nel, A.: A high-precision fluid handling system based on pressure actuation: multi-inlets flow rate control. In: Proc. 3rd Eur. Conf. Microfluidics, vol. 252 (2012)

[41] Wong, Y.H.: Feedback controls in droplet microfluidics. Master's thesis, University of Waterloo (2016)

[42] Hébert, M., Courtney, M., Ren, C.L.: Semi-automated on-demand control of individual droplets with a sample application to a drug screening assay. Lab on a Chip (2019)

[43] Wong, D., Erkorkmaz, K., Ren, C.L.: Robodrop: A multi-input multi-output control system for on-demand manipulation of microfluidic droplets based on computer vision feedback. IEEE/ASME Transactions on Mechatronics **25**(2), 1129–1137 (2020)

[44] Ljung, L.: System Identification: Theory for the User. Pearson Education, ??? (1998). https://books.google.ca/books?id=fYSrk4wDKPsC

[45] Bazanella, A.S., Gevers, M., Miškovic, L.: Closed-loop identification of mimo systems: a new look at identifiability and experiment design. European Journal of Control **16**(3), 228–239 (2010)

[46] Gábor, A., Villaverde, A.F., Banga, J.R.: Parameter identifiability analysis and visualization in large-scale kinetic models of biosystems. BMC systems biology **11**(1), 54 (2017)

[47] Brun, R., Reichert, P., Künsch, H.R.: Practical identifiability analysis of large environmental simulation models. Water Resources Research **37**(4), 1015–1030 (2001)

[48] Christov, I.C., Cognet, V., Shidhore, T.C., Stone, H.A.: Flow rate–pressure drop relation for deformable shallow microfluidic channels. Journal of Fluid Mechanics **841**, 267–286 (2018)

[49] Norton, J.P.: An Introduction to Identification. Courier Corporation, ??? (2009)

[50] Hébert, M., Baxter, W., Huissoon, J.P., Ren, C.L.: A quantitative study of the dynamic response of soft tubing for pressure-driven flow in a microfluidics context. Microfluidics and Nanofluidics **24**(12), 1–13 (2020)

[51] Montgomery, D.C., Runger, G.C.: Applied Statistics and Probability for Engineers. John Wiley & Sons, ??? (2010)

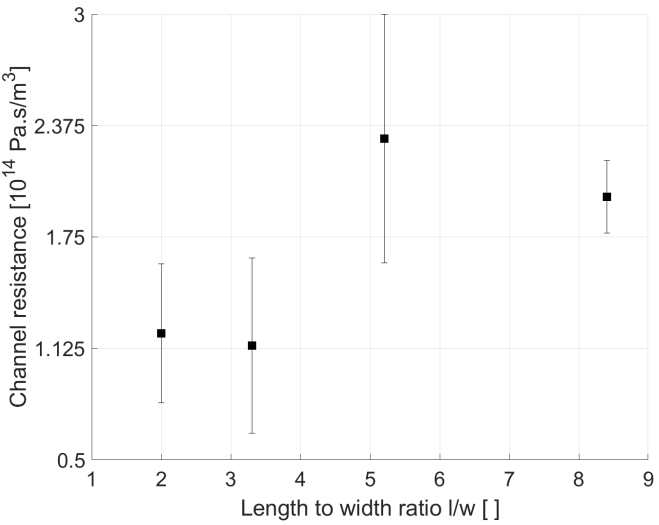

(a) Identified channel resistance for droplet-length-to-channel-width ratios with the error bars corresponding to one standard deviation.

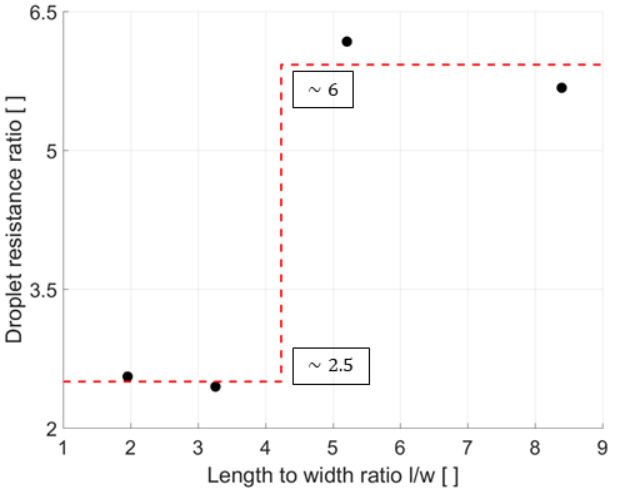

(b) Ratio of experimental to theoretical (i.e. single-phase) droplet resistance according to Equation 11.

Fig. 10 Experimental droplet resistance results.